Published in final edited form as:
J Magn Reson Imaging. 2008 May ; 27(5): 1069–1076. doi:10.1002/jmri.21327.

Diffusion-Weighted PROPELLER MRI for Quantitative Assessment of Liver Tumor Necrotic Fraction and Viable Tumor Volume in VX2 Rabbits

Jie Deng, MS[1,2], **Sumeet Virmani, MD**[1], **Joseph Young, BS**[1], **Kathleen Harris, BS**[1], **Guang-Yu Yang, MD**[3], **Alfred Rademaker, PhD**[4], **Gayle Woloschak, PhD**[5,6], **Reed A. Omary, MD**[1,2,6], and **Andrew C. Larson, PhD**[1,2,6,*]

[1]Department of Radiology, Northwestern University, Chicago, Illinois.

[2]Department of Biomedical Engineering, Northwestern University, Chicago, Illinois.

[3]Department of Pathology, Northwestern University, Chicago, Illinois.

[4]Department of Preventive Medicine, Northwestern University, Chicago, Illinois.

[5]Department of Radiation Oncology, Northwestern University, Chicago, Illinois.

[6]Feinberg School of Medicine, Robert H. Lurie Comprehensive Cancer Center, Northwestern University, Chicago, Illinois.

Abstract

Purpose—To test the hypothesis that diffusion-weighted (DW)-PROPELLER (periodically rotated overlapping parallel lines with enhanced reconstruction) MRI provides more accurate liver tumor necrotic fraction (NF) and viable tumor volume (VTV) measurements than conventional DW-SE-EPI (spin echo echo-planar imaging) methods.

Materials and Methods—Our institutional Animal Care and Use Committee approved all experiments. In six rabbits implanted with 10 VX2 liver tumors, DW-PROPELLER and DW-SE-EPI scans were performed at contiguous axial slice positions covering each tumor volume. Apparent diffusion coefficient maps of each tumor were used to generate spatially resolved tumor viability maps for NF and VTV measurements. We compared NF, whole tumor volume (WTV), and VTV measurements to corresponding reference standard histological measurements based on correlation and concordance coefficients and the Bland–Altman analysis.

Results—DW-PROPELLER generally improved image quality with less distortion compared to DW-SE-EPI. DW-PROPELLER NF, WTV, and VTV measurements were strongly correlated and satisfactorily concordant with histological measurements. DW-SE-EPI NF measurements were weakly correlated and poorly concordant with histological measurements. Bland–Altman analysis demonstrated that DWPROPELLER WTV and VTV measurements were less biased from histological measurements than the corresponding DW-SE-EPI measurements.

Conclusion—DW-PROPELLER MRI can provide spatially resolved liver tumor viability maps for accurate NF and VTV measurements, superior to DW-SE-EPI approaches. DWPROPELLER measurements may serve as a noninvasive surrogate for pathology, offering the potential for more accurate assessments of therapy response than conventional anatomic size measurements.

Please send correspondence and reprint requests to: Andrew C. Larson, Northwestern University, Department of Radiology, 737 N Michigan Ave, Suite 1600, Chicago, IL 60611, Tel: (312) 926-3499 Fax: (312)926-5991, a-larson@northwestern.edu.

Keywords

diffusion-weighted imaging; PROPELLER; liver tumor; necrosis; viability

PATIENTS WITH LIVER TUMORS of primary or metastatic origin can undergo a number of potential therapies. Accurate, timely assessment of response is critical to individualize treatment regimens. Anatomic tumor size changes as specified by the Response Evaluation Criteria in Solid Tumors (RECIST) (1) or World Health Organization (WHO) criteria (2) are most commonly used to evaluate response. However, liver tumor response often involves the formation of necrosis without immediate size changes. A noninvasive surrogate for pathology providing necrotic fraction (NF), whole-tumor- volume (WTV), and viable-tumor-volume (VTV) measurements would permit more accurate assessments of therapy response. Accordingly, the European Association for the Study of Liver Disease (EASL) recently proposed measuring posttherapy changes in VTV with contrast-enhanced (CE) CT or MRI (3,4). However, CE CT and MRI measurements may struggle to accurately differentiate viable from necrotic tissues (5–10) and to our knowledge have yet to be validated for VTV measurements in liver tumors.

Alternatively, diffusion-weighted MRI (DWI) may permit tissue characterization without the need for exogenous contrast agents. DWI uses local water mobility as an endogenous probe for noninvasive interrogation of tissue microstructure. DWI has been used for detection of liver tumors (11), differentiation of lesion types (12), and detection of microstructural changes after therapy (13). DWI offers the potential to differentiate viable tissues from regions of necrosis based on the difference in local water mobility between these tissues (14). Previous studies demonstrated a strong correlation between tumor NF and mean whole tumor apparent diffusion coefficient (ADC) measurements (15–17). More recently, Carano et al (18) and Henning et al (19) each used DWI to generate spatially resolved tissue viability maps for VTV measurements in murine xenograft human colon and RIF-1 tumor models, respectively. However, to our knowledge no studies have used DWI for in situ VTV or NF measurements in liver tumors.

Production of spatially resolved liver tumor viability maps with conventional single-shot DW-SE-EPI approaches may be challenging. Particularly for abdominal applications, single-shot approaches often result in relatively poor overall image quality due to geometric distortion, chemical shift artifacts, and limited spatial resolution (20). Multishot DWI approaches may overcome these limitations (21–24). Multishot DW-PROPELLER (periodically rotated overlapping parallel lines with enhanced reconstruction) approaches were less sensitive to motion artifacts due to the intrinsic properties of segmental phase corrections and oversampling at the central k-space. A recent study using multishot DW-PROPELLER demonstrated significantly improved image quality for abdominal DWI with reduced distortion and artifact levels compared to DW-SE-EPI (25).

The purpose of our study was to compare DW-SE-EPI and DW-PROPELLER NF and VTV measurements to reference standard histological measurements in a rabbit VX2 liver tumor model. We tested the hypothesis that DW-PROPELLER provides more accurate liver tumor NF and VTV measurements than conventional DW-SE-EPI.

MATERIALS AND METHODS

Animal Model

Our institutional Animal Care and Use Committee approved all experiments. Six 4–5 kg New Zealand white rabbits were used for these experiments. VX2 cells were initially grown

in the hindlimb of donor rabbits. A small incision was made in the hepatic capsule of each rabbit and harvested tumor portions with 2mmdiameter were implanted during a mini-laparotomy procedure (26). In six rabbits a total of 10 VX2 liver tumors were included and allowed to grow for 3–4 weeks before imaging (diameter ranging from 1.1–2.5 cm).

MRI

MRI was performed using a 1.5T Magnetom Sonata clinical scanner (Siemens Medical Solutions, Erlangen, Germany). Rabbits were intubated with a 3 French endotracheal tube and administered isofluorane anesthesia with a small animal ventilator (Harvard Apparatus, Holliston, MA) throughout imaging procedures (60–70 breaths/min). Rabbits were imaged in the supine position using a clinical head coil. Respiratory gating was accomplished using a pneumatic bellows belt strapped about the lower abdomen of each rabbit.

Following initial localization scans, DW images were acquired using single-shot DW-SE-EPI (14) and multishot DW-PROPELLER sequences (25) at identical, contiguous axial slice positions providing complete coverage of each liver tumor (5–10 slices were acquired based on each tumor size). Single-shot DW-SE-EPI parameters were: TR/TE = 3600/86 msec, 1.5 kHz/pixel readout BW, 15.6 Hz/pixel phase BW, 200 × 137.5 mm^2 FOV, 128 × 88 matrix (1.6 × 1.6 × 3.0 mm^3), 5/8 partial-Fourier, EPI factor = 88, six signal averages, nonselective fat saturation, twice refocused spin-echo diffusion preparation. Multishot DW-PROPELLER parameters were: TR/TE = 3600/68 msec, 400 Hz/pixel readout BW, 200 × 200 mm^2 FOV, 128 × 128 matrix (1.6 × 1.6 × 3.0 mm3), ETL = 17, 60 segments, nonselective fat saturation. Our implemented DW-PROPELLER pulse sequence was based on the BLADE pulse sequence (Siemens Medical Solutions implementation of PROPELLER TSE). Motion probing gradients separated by a slice-selective 180° refocusing pulse provided the requisite diffusion weighting. For both DWI sequences, images at diffusion weightings of b = 0, 500, and 1000 s/mm^2 were acquired (DW applied along inplane left/right orientation). Based on the current acquisition parameters the imaging time for multishot DW-PROPELLER method was 3.5 minutes for each DW image and totally around 11 minutes for all DW images at three b values; the imaging time for the single-shot DW-SE-EPI method was round 1 minute for all DW images.

Image Analysis

Postprocessing was performed offline using MatLab software (MathWorks, Natick, MA). For both DWI sequences, ADC maps were generated on a pixel-by-pixel basis at each axial slice position that included tumor tissues. A tumor region-of-interest (ROI) was manually selected at each slice position (drawn upon b = 1000 s/mm^2 DWI) and transferred to the corresponding ADC map. The ADC values of all voxels within the entire tumor volume were classified into two tissue populations using the *K*-means (KM) clustering algorithm (18,19,27). High and low ADC populations were assumed to represent necrotic and viable tissues. These were depicted as bright and dark voxels, respectively, within our spatially resolved liver tumor viability maps. Whole tumor NF was calculated by dividing the total number of necrotic voxels by the total number of voxels included within the tumor ROIs. WTV was calculated by multiplying the voxel volume by the total number of voxels included within the tumor ROIs. VTV was calculated by multiplication of WTV by the viable tumor fraction (1-NF).

Histological Analysis

After removal from the scanner bore, each rabbit was euthanized with commercial intravenous Beuthanasia solution containing pentobarbital (100 mg/kg) and rabbit livers were harvested for subsequent necropsy. Livers were fixed in 10% buffered formaldehyde solution and sliced at 3-mm intervals in the axial plane to correspond to the plane of the MR

images. Tumor nodules were embedded in paraffin for histological examination. These nodules were sliced in 4-μm thick sections and stained using hematoxylin and eosin (H&E) to confirm tumor necrosis. Histological slides were digitized with ×40 optical magnification using a multispectral imaging system (Nuance, CRI, Woburn, MA). Magnified portions were stitched together for simultaneous inspection of complete tumor slices (PanaVue ImageAssembler, QC, Canada). H&E cell staining and cell morphology were characterized by an attending pathologist. For each histology slide, ImageJ software (NIH, Bethesda, MD) was used to manually circumscribe outer tumor borders and regions of tumor necrosis (Fig. 1). For each tumor, histological NF was calculated by dividing the total pixel areas included in necrotic regions by the total pixel areas included within the tumor border (across all slices). WTV was calculated by multiplying the total pixel areas included within the tumor borders by the slice thickness. VTV was calculated by multiplication of WTV by the histologically determined viable tumor fraction (1-NF). Finally, a whole volumetric shrinkage scale was calculated as the difference between DWI WTV and histopathology WTV divided by DWI WTV.

Statistical Analysis

We compared DWI NF, WTV, and VTV measurements to reference standard histological measurements. First, we calculated the linear correlation between each set of DWI measurements and each corresponding set of histological measurements (Pearson's correlation coefficient r). Next, separately for NF, WTV, and VTV measurements, we used a modified t-test (28) to determine whether there was a significant difference between the correlation coefficients calculated for DW-SE-EPI and DW-PROPELLER measurements. For all comparisons $P < 0.05$ was considered statistically significant.

Separately, for each of the two DWI techniques, we also calculated Lin's concordance coefficient (r_c) to determine whether the data from the two sources (each set of DWI and histological measurements) fell upon a 45° line of identity, ie, whether the data were totally reproducible between the two sources (29). Lin's concordance coefficient combines measures of both precision and accuracy to determine whether the observed data deviate significantly from perfect concordance. Excellent agreement was considered $r_c > 0.9$, satisfactory $0.6 < r_c < 0.9$, unsatisfactory $r_c < 0.6$ (29,30).

Additionally, we generated Bland–Altman plots for each set of measurements (31) to further investigate the agreement between DWI and histological measurements. The bias was estimated by calculating the mean and standard deviation (SD) of the differences between DWI and histological measurements for each dataset. The limits of agreement were calculated as the interval of differences between mean ± 1.96 SD. A lower limit of agreement represents higher agreement between two measurement methods.

Mean ADC values of viable and necrotic tissues as classified from a tumor viability map in each rabbit were calculated for both single-shot DW-SE-EPI and multishot DW-PROPELLER techniques. A matched pair t-test was used (2-tailed, $P < 0.05$) to test for statistical difference of mean ADC between viable and necrotic tumor tissue measured by each of the DWI techniques and to test for statistical difference of mean ADC of each tissue type between the two DWI techniques.

RESULTS

Representative examples of DW-SE-EPI and DW-PROPELLER images with corresponding ADC maps at the center of VX2 liver tumors are shown in Fig. 2 and 3. Each tumor was clearly differentiated on the T2-weighted $b = 0$ images with greater relative signal intensity within tumor tissues compared to surrounding normal liver parenchyma. With increasing b

value, necrotic tumor cores demonstrated greater signal suppression than the peripheral viable tumor tissues. Qualitatively, intratumoral tissue heterogeneity was better represented on DW images with $b = 1000$. Necrotic tumor tissues, primarily within the central tumor core, resulted in elevated ADC values compared to the reduced ADC values within peripheral viable tissues.

No obvious motion artifacts were present within the DW images. As shown in Fig. 2, DW-PROPELLER images clearly depict a viable tumor rim surrounding a central necrotic core. The DW-PROPELLER $b = 0$ image contained sharp tumor borders and surrounding anatomic structures, while the DW-SE-EPI $b = 0$ image was blurred and mildly distorted. For the DW-PROPELLER tumor viability map, intratumoral necrotic and viable tissue classifications were well correlated to H&E histopathology. For the DW-SE-EPI tumor viability map the necrotic tumor region was overestimated in the anterior region, possibly due to blurring of the DW-SE-EPI images along the phase-encoding dimension (anterior–posterior orientation). For the example shown in Fig. 3, both DW-PROPELLER and DW-SE-EPI images clearly differentiated tumor regions from the normal liver parenchyma. For this example the classification of tissue types within both DW-PROPELLER and DW-SE-EPI viability maps were well correlated to H&E histopathology. A specific example comparing high-quality DWPROPELLER images to particularly poor quality DW-SE-EPI images is shown in Fig. 4. For this rabbit a local field inhomogeneity, arising from tissue–air interfaces near the tumor position, led to severe image distortion and signal loss. DW-PROPELLER, by comparison, provided undistorted images of superior quality.

As shown in Fig. 5a, DW-SE-EPI NF measurements were not well correlated to histological NF measurements ($r = 0.33$, $P = 0.35$), whereas DW-PROPELLER NF measurements were highly correlated to histopathology ($r = 0.87$, $P = 0.001$). The difference between these DW-SE-EPI and DW-PROPELLER correlation coefficients were statistically significant ($P = 0.04$). Concordance of DW-SE-EPI ($r_c = 0.24$, 95% confidence interval [CI] = [−0.25, 0.63], $P = 0.17$) measurements was not statistically greater than zero. Concordance of DWPROPELLER ($r_c = 0.87$, 95% CI = [0.57, 0.97], $P < 0.0001$) measurements was statistically significant and greater than the 0.6 cutoff level considered satisfactory for precise agreement. Figure 5d shows the Bland–Altman comparison of DW-PROPELLER and DW-SE-EPI NF measurements to histological NF measurements. The mean difference was 0 for DW-PROPELLER with 95% CI [−0.034, 0.034] compared to mean difference 0.059 for DW-SE-EPI with 95% CI [0.009, 0.13]. The limits of agreement (−0.094 to 0.094) for DW-PROPELLER were lower than those for DW-SEEPI (−0.128 to 0.246).

As shown in Fig. 5b, both DW-SE-EPI and DW-PROPELLER WTV measurements were highly correlated to histological WTV measurements ($r = 0.89$, $P = 0.0005$ and $r = 0.90$, $P = 0.0004$, respectively). The difference between these DW-SE-EPI and DW-PROPELLER correlation coefficients were not statistically significant ($P = 0.88$). Concordance of DW-SE-EPI ($r_c = 0.49$, 95% CI = [0.17, 0.72], $P = 0.002$) and DW-PROPELLER ($r_c = 0.63$, 95% CI = [0.28, 0.84], $P = 0.0007$) WTV measurements to histopathology measurements were both significantly greater than zero. However, only the DW-PROPELLER WTV r_c value was greater than the 0.6 cutoff level considered satisfactory for precise agreement. All DW-SE-EPI and DW-PROPELLER WTV measurements were larger than corresponding histological WTV measurements. However, volumetric shrinkage scales for both DW-SE-EPI and DW-PROPELLER (38 ± 14% and 31 ± 12%, mean ± SD, respectively) were consistent with previously reported studies (32). As shown in the Bland–Altman plot (Fig. 5e), the mean difference was 580.5 mm^3 for DW-PROPELLER with 95% CI [360.7, 800.3] mm^3, which were smaller than those measured by DW-SE-EPI (mean difference 889.8 mm^3 with 95% CI [459.5, 1320.1] mm^3). The limits of agreement (−21.8 mm^3 to 1182.8 mm^3) for DW-PROPELLER were smaller than those for DW-SE-EPI (−289.3 mm^3 to 2068.9 mm^3).

As shown in Fig. 5c, both DW-SE-EPI and DW-PROPELLER VTV measurements were correlated to histological measurements ($r = 0.80$, $P = 0.005$ and $r = 0.93$, $P = 0.0001$, respectively). While the correlation coefficient r was greater for the DW-PROPELLER measurements, the difference between DW-SE-EPI and DW-PROPELLER correlation coefficients did not achieve statistical significance ($P = 0.10$). Concordance of both DW-SE-EPI ($r_c = 0.56$, 95% CI = [0.16, 0.80], $P = 0.004$) and DW-PROPELLER ($r_c = 0.71$, 95% CI = [0.38, 0.88], $P = 0.0002$) VTV measurements to histopathology were both significantly greater than zero. However, only the DW-PROPELLER VTV r_c value was greater than the 0.6 cutoff level considered satisfactory for precise agreement. Figure 5f shows the Bland–Altman comparison of DW-PROPELLER and DW-SE-EPI VTV measurements to histological VTV measurements. All DW-SE-EPI and DW-PROPELLER VTV measurements were larger than corresponding histological VTV measurements. The mean difference was 398.9 mm^3 for DW-PROPELLER with 95% CI [252.6, 545.2] mm^3, which were smaller than those measured by DW-SE-EPI (mean difference 513.2 mm^3 with 95% CI [87.3, 839.3] mm^3). The limits of agreement (-1.8 mm^3 to 799.6 mm^3) for DW-PROPELLER were smaller than those for DW-SE-EPI (-380.2 mm^3 to 1406.6 mm^3).

For all 10 tumors the mean ADC of viable tumor tissues was $(1.53 \pm 0.20) \times 10^{-3}$ mm^2/s measured by DW-PROPELLER and $(0.91 \pm 0.20) \times 10^{-3}$ mm^2/s measured by DW-SE-EPI. The mean ADC of tumor necrosis were $(2.37 \pm 0.47) \times 10^{-3}$ mm^2/s measured by DW-PROPELLER and $(1.49 \pm 0.40) \times 10^{-3}$ mm^2/s measured by DW-SE-EPI. The difference of mean ADC between viable and necrotic tumor tissues measured by each of the DWI techniques was significant ($P < 1 \times 10^{-5}$). However, the mean ADCs of viable and necrotic tumor tissues measured by DW-PROPELLER were generally greater than those measured by DW-SE-EPI ($P < 1 \times 10^{-6}$).

DISCUSSION

Quantitative evaluation of liver tumor viability may be critical to permit accurate, timely assessment of therapy response. Our preclinical studies demonstrate the feasibility of using DWI as a noninvasive imaging surrogate for liver tumor histopathology. We were able to generate spatially resolved tissue viability maps for in vivo measurements of VX2 liver tumor NF and VTV. DWI measurements, particularly those obtained using DW-PROPELLER, were strongly correlated and satisfactorily concordant with histopathology. To our knowledge this study represents the first use of DWI for in situ spatially resolved quantification of liver tumor NF and VTV. DW-PROPELLER tumor viability measurements may offer an important alternative to conventional anatomic size measurements for assessing therapeutic response. For our study DW-PROPELLER NF, WTV, and VTV measurements were each strongly correlated and satisfactorily concordant with histological measurements. The higher agreement between DW-PROPELLER and histology NF measurements were considered small enough to consider that DW-PROPELLER can be used as an imaging surrogate for tumor NF measurements. DW-SE-EPI NF measurements were only weakly correlated and poorly concordant with histological NF measurements. The low agreement between DW-SE-EPI and histology NF measurements indicated that DW-SE-EPI was not acceptable as an accurate method for NF measurements. However, the correlation of DW-SE-EPI VTV measurements to histology was not significantly different from the correlation of DW-PROPELLER measurements ($P = 0.10$). This was unexpected, given the poor correlation of DW-SE-EPI NF measurements to histopathology. The moderately high correlation of DW-SE-EPI VTV measurements may simply result from the strong correlation of DW-SE-EPI to histological WTV measurements. However, given the current trend, with a larger sample size we would expect to achieve statistical significance between the correlations of DW-PROPELLER and DW-SE-EPI VTV measurements to histological VTV measurements. DW-SE-EPI NF, WTV, and VTV measurements were not

satisfactorily concordant with corresponding histological measurements. Additionally, all DWI WTV and VTV measurements were generally higher than histology measurements. These overestimations are due to the tissue shrinkage caused by 10% formalin fixation and by dehydration, clearance, and paraffin wax embedding. Despite this, the mean differences and the limits of agreement between DW-PROPELLER and histology WTV and VTV measurements were smaller than those between DW-SE-EPI and histology measurements. Overall, the results of our study validate that DW-PROPELLER is more accurate than conventional DW-SE-EPI for in situ quantification of liver tumor viability.

The discordance of ADC measurements between DWPROPELLER and DW-SE-EPI could be attributed to several possible reasons. 1) Previous liver DWI studies reported that ADC measurements increased during nonbreath-hold acquisitions (33) and multishot DWPROPELLER ADC measurements may be more sensitive to motion than single-shot DW-SE-EPI approaches. 2) Diffusion time (t_{diff}) in two diffusion preparation schemes was different (ie, DW-PROPELLER t_{diff} ~20 ms and DW-EPI t_{diff} ~ 45 ms). Within a short tdiff range, increased tdiff may lead to restricted diffusion and decreased ADC (34). 3) Signal-to-noise ratio (SNR) differences between these single-shot and multishot sequences may lead to different ADC measurements. However, even though DW-PROPELLER ADC measurements with our current implementation were higher than the expected ADC values measured using single shot DW-SE-EPI, DW-PROPELLER still achieved superior accuracy in tumor tissue classification for differentiation of viable from necrotic tumor tissues.

For decades radiological evaluation of anatomic size change has been the reference standard for the assessment of liver tumor response. The considerable limitations of these anatomic approaches, particularly in the setting of liver-directed therapies, recently lead the EASL to suggest measuring viable tumor volume rather than overall tumor size changes (3). However, the recommended CE imaging methods may struggle to accurately differentiate viable from necrotic tumor tissues (5–7). Extravasation of contrast agent with subsequent diffusion into neighboring necrotic tissues may lead to overestimation of viable volumes or, conversely, hypoxic viable tumor tissues with limited patent vasculature may not receive detectable levels of contrast agent leading to underestimation of viable tumor volume. Dynamic CE (DCE) pharmacokinetic measurements may more accurately discriminate viable and necrotic tissues (8,36) but these approaches have yet to be validated, to our knowledge, for liver tumors. DWI offers an alternative functional imaging approach permitting direct interrogation of tumor tissue structure without the need for exogenous contrast agents. Most previous DWI studies measured gross functional changes attributed to the entire tumor volume (15–17). Such assessments would inherently mask heterogeneous intratumoral tissue alterations and direct clinical interpretation of mean whole tumor ADC measurements may be difficult as opposed to interpretation of surrogate DWI VTV or NF measurements.

Carano et al (18) and more recently Henning et al (19) each proposed multidimensional approaches combining ADC, T2, and spin-density measurements to produce spatially resolved tumor viability maps in subcutaneous xenograft murine tumor models. These approaches provided VTV and NF measurements closely correlated to histopathology derived measurements. For both of these studies, tissue ADC was the dominant parameter for intratumoral tissue classification. However, a combination of ADC, T2, and/or spindensity measurements provided the most accurate VTV measurements. In future studies the addition of quantitative T2 and spin-density measurements to our current DW-PROPELLER ADC measurements may also improve the accuracy of liver tumor NF and VTV measurements. The aforementioned studies in xenograft murine models were the first to describe in vivo DWI techniques for the production of spatially resolved tumor viability maps. Our subsequent contribution has been to develop and validate abdominal DW-

PROPELLER techniques for in situ derivation of spatially resolved liver tumor viability maps using a clinical MRI scanner. Implementation and validation of our techniques on a clinical scanner should facilitate our planned translational studies to evaluate the accuracy of clinical DWI NF and VTV measurements in liver cancer patients before and after therapy.

The primary limitation of our study was the lack of comparisons to conventional CE imaging approaches. A secondary limitation of our study was the lack of serial, longitudinal NF and VTV measurements after therapy. VX2 rabbits provide a useful model for VTV and NF measurements independent of therapy because as each VX2 tumor grows, necrotic regions are formed due to central hypoxic conditions within each tumor. However, future studies are needed to assess the accuracy of DWI NF and VTV measurements after therapies that induce tissue necrosis via alternate cell death pathways.

In conclusion, DW-PROPELLER MRI can provide spatially resolved liver tumor viability maps for NF and VTV measurements. DW-PROPELLER NF and VTV measurements were closely correlated and satisfactorily concordant with histology and superior to DW-SE-EPI measurements. DW-PROPELLER measurements can serve as a noninvasive surrogate for pathology offering the potential for more accurate assessments of therapy response than conventional anatomic size measurements.

Acknowledgments

The authors thank Tatjana Paunesku for expert assistance with VX2 tumor cell culture and Richard Tang for animal model preparation and handling during MRI. Also, we wish to thank Alto Stemmer of Siemens Medical Solutions, Erlangen, Germany, for providing access to his BLADE-TSE sequence source codes.

REFERENCES

1. Therasse P, Arbuck SG, Eisenhauer EA, et al. New guidelines to evaluate the response to treatment in solid tumors. European Organization for Research and Treatment of Cancer, National Cancer Institute of the United States, National Cancer Institute of Canada. J Natl Cancer Inst 2000;92:205–216. [PubMed: 10655437]
2. Miller AB, Hoogstraten B, Staquet M, Winkler A. Reporting results of cancer treatment. Cancer 1981;47:207–214. [PubMed: 7459811]
3. Bruix J, Sherman M, Llovet JM, et al. Clinical management of hepatocellular carcinoma. Conclusions of the Barcelona-2000 EASL conference. European Association for the Study of the Liver. J Hepatol 2001;35:421–430. [PubMed: 11592607]
4. Llovet JM, Beaugrand M. Hepatocellular carcinoma: present status and future prospects. J Hepatol 2003;38 suppl 1:S136–S149. [PubMed: 12591191]
5. Erlemann R, Sciuk J, Bosse A, et al. Response of osteosarcoma and Ewing sarcoma to preoperative chemotherapy: assessment with dynamic and static MR imaging and skeletal scintigraphy. Radiology 1990;175:791–796. [PubMed: 2188300]
6. Furman-Haran E, Margalit R, Grobgeld D, Degani H. Dynamic contrast-enhanced magnetic resonance imaging reveals stress-induced angiogenesis in MCF7 human breast tumors. Proc Natl Acad Sci U S A 1996;93:6247–6251. [PubMed: 8692800]
7. Lang P, Wendland MF, Saeed M, et al. Osteogenic sarcoma: noninvasive in vivo assessment of tumor necrosis with diffusion-weighted MR imaging. Radiology 1998;206:227–235. [PubMed: 9423677]
8. Dyke JP, Panicek DM, Healey JH, et al. Osteogenic and Ewing sarcomas: estimation of necrotic fraction during induction chemotherapy with dynamic contrast-enhanced MR imaging. Radiology 2003;228:271–278. [PubMed: 12832588]
9. Uhl M, Saueressig U, van Buiren M, et al. Osteosarcoma: preliminary results of in vivo assessment of tumor necrosis after chemotherapy with diffusion- and perfusion-weighted magnetic resonance imaging. Invest Radiol 2006;41:618–623. [PubMed: 16829744]

10. Broumas AR, Pollard RE, Bloch SH, Wisner ER, Griffey S, Ferrara KW. Contrast-enhanced computed tomography and ultrasound for the evaluation of tumor blood flow. Invest Radiol 2005;40:134–147. [PubMed: 15714088]
11. Takahara T, Imai Y, Yamashita T, Yasuda S, Nasu S, Van Cauteren M. Diffusion weighted whole body imaging with background body signal suppression (DWIBS): technical improvement using free breathing, STIR and high resolution 3D display. Radiat Med 2004;22:275–282. [PubMed: 15468951]
12. Namimoto T, Yamashita Y, Sumi S, Tang Y, Takahashi M. Focal liver masses: characterization with diffusion-weighted echo-planar MR imaging. Radiology 1997;204:739–744. [PubMed: 9280252]
13. Geschwind JF, Artemov D, Abraham S, et al. Chemoembolization of liver tumor in a rabbit model: assessment of tumor cell death with diffusion-weighted MR imaging and histologic analysis. J Vasc Interv Radiol 2000;11:1245–1255. [PubMed: 11099235]
14. Deng J, Rhee TK, Sato KT, et al. In vivo diffusion-weighted imaging of liver tumor necrosis in the VX2 rabbit model at 1.5 Tesla. Invest Radiol 2006;41:410–414. [PubMed: 16523024]
15. Kamel IR, Bluemke DA, Ramsey D, et al. Role of diffusion-weighted imaging in estimating tumor necrosis after chemoembolization of hepatocellular carcinoma. AJR Am J Roentgenol 2003;181:708–710. [PubMed: 12933464]
16. Lyng H, Haraldseth O, Rofstad EK. Measurement of cell density and necrotic fraction in human melanoma xenografts by diffusion weighted magnetic resonance imaging. Magn Reson Med 2000;43:828–836. [PubMed: 10861877]
17. Helmer KG, Meiler MR, Sotak CH, Petruccelli JD. Comparison of the return-to-the-origin probability and the apparent diffusion coefficient of water as indicators of necrosis in RIF-1 tumors. Magn Reson Med 2003;49:468–478. [PubMed: 12594749]
18. Carano RA, Ross AL, Ross J, et al. Quantification of tumor tissue populations by multispectral analysis. Magn Reson Med 2004;51:542–551. [PubMed: 15004796]
19. Henning EC, Azuma C, Sotak CH, Helmer KG. Multispectral quantification of tissue types in a RIF-1 tumor model with histological validation. Part I. Magn Reson Med 2007;57:501–512. [PubMed: 17326181]
20. Farzaneh F, Riederer SJ, Pelc NJ. Analysis of T2 limitations and off-resonance effects on spatial resolution and artifacts in echoplanar imaging. Magn Reson Med 1990;14:123–139. [PubMed: 2352469]
21. Pipe JG, Farthing VG, Forbes KP. Multishot diffusion-weighted FSE using PROPELLER MRI. Magn Reson Med 2002;47:42–52. [PubMed: 11754441]
22. Trouard TP, Theilmann RJ, Altbach MI, Gmitro AF. High-resolution diffusion imaging with DIFRAD-FSE (diffusion-weighted radial acquisition of data with fast spin-echo) MRI. Magn Reson Med 1999;42:11–18. [PubMed: 10398944]
23. Butts K, de Crespigny A, Pauly JM, Moseley M. Diffusion-weighted interleaved echo-planar imaging with a pair of orthogonal navigator echoes. Magn Reson Med 1996;35:763–770. [PubMed: 8722828]
24. Gudbjartsson H, Maier SE, Mulkern RV, Morocz IA, Patz S, Jolesz FA. Line scan diffusion imaging. Magn Reson Med 1996;36:509–519. [PubMed: 8892201]
25. Deng J, Miller FH, Salem R, Omary RA, Larson AC. Multishot diffusion-weighted PROPELLER magnetic resonance imaging of the abdomen. Invest Radiol 2006;41:769–775. [PubMed: 16971801]
26. Wang D, Bangash A, Rhee TK, et al. Transcatheter intraarterial first-pass perfusion (TRIP) — MRI monitoring of liver tumor embolization in VX2 rabbits. Radiology. 2007 (in press).
27. Bezdek JC, Hall LO, Clarke LP. Review of MR image segmentation techniques using pattern recognition. Med Phys 1993;20:1033–1048. [PubMed: 8413011]
28. Chen, PY.; Popovich, PM. Covers tests of difference between two dependent correlations, and the difference between more than two independent correlations. Thousand Oaks, CA: Sage Publications; 2002. Correlation: parametric and nonparametric measures.
29. Lin LI. A concordance correlation coefficient to evaluate reproducibility. Biometrics 1989;45:255–268. [PubMed: 2720055]

30. Warke TJ, Kamath S, Fitch PS, Brown V, Shields MD, Ennis M. The repeatability of nonbronchoscopic bronchoalveolar lavage differential cell counts. Eur Respir J 2001;18:1009–1012. [PubMed: 11829083]

31. Bland JM, Altman DG. Statistical methods for assessing agreement between two methods of clinical measurement. Lancet 1986;1:307–310. [PubMed: 2868172]

32. Kinoshita Y, Okudera T, Tsuru E, Yokota A. Volumetric analysis of the germinal matrix and lateral ventricles performed using MR images of postmortem fetuses. AJNR Am J Neuroradiol 2001;22:382–388. [PubMed: 11156787]

33. Sandberg A, Parikh T, Johnson G, Stemmer A, Xu J, Taouli B. Feasibility of a respiratory-triggered SSEPI diffusion-weighted sequenc for liver imaging using navigator echo technique: comparison with breath-hold diffusion-weighted sequence. Proc ISMRM 2006;14

34. Pfeuffer J, Flogel U, Dreher W, Leibfritz D. Restricted diffusion and exchange of intracellular water: theoretical modelling and diffusion time dependence of 1H NMR measurements on perfused glial cells. NMR Biomed 1998;11:19–31. [PubMed: 9608585]

35. Ross BD, Moffat BA, Lawrence TS, et al. Evaluation of cancer therapy using diffusion magnetic resonance imaging. Mol Cancer Ther 2003;2:581–587. [PubMed: 12813138]

36. Benjaminsen IC, Graff BA, Brurberg KG, Rofstad EK. Assessment of tumor blood perfusion by high-resolution dynamic contrastenhanced MRI: a preclinical study of human melanoma xenografts. Magn Reson Med 2004;52:269–276. [PubMed: 15282808]

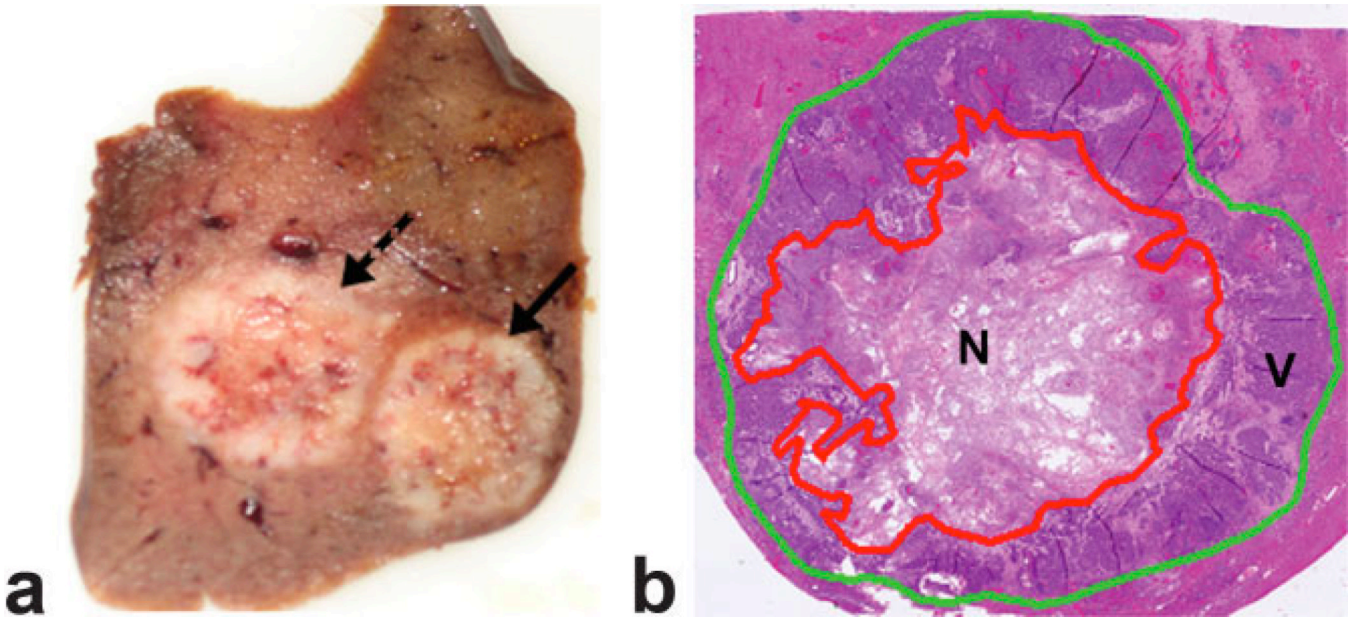

Figure 1.

a: Axial view of a 3-mm thick slice of rabbit liver specimen including two VX2 tumors (solid arrow and dashed arrow) and surrounding normal hepatic parenchyma. **b:** Composite H&E histology image of the rightmost tumor (solid arrow within a) for simultaneous inspection of the entire tumor. For each pathology image both an outer tumor border (green line) and inner regions of necrosis (red line) were manually circumscribed to permit reference standard histopathology-based NF and VTV measurements.

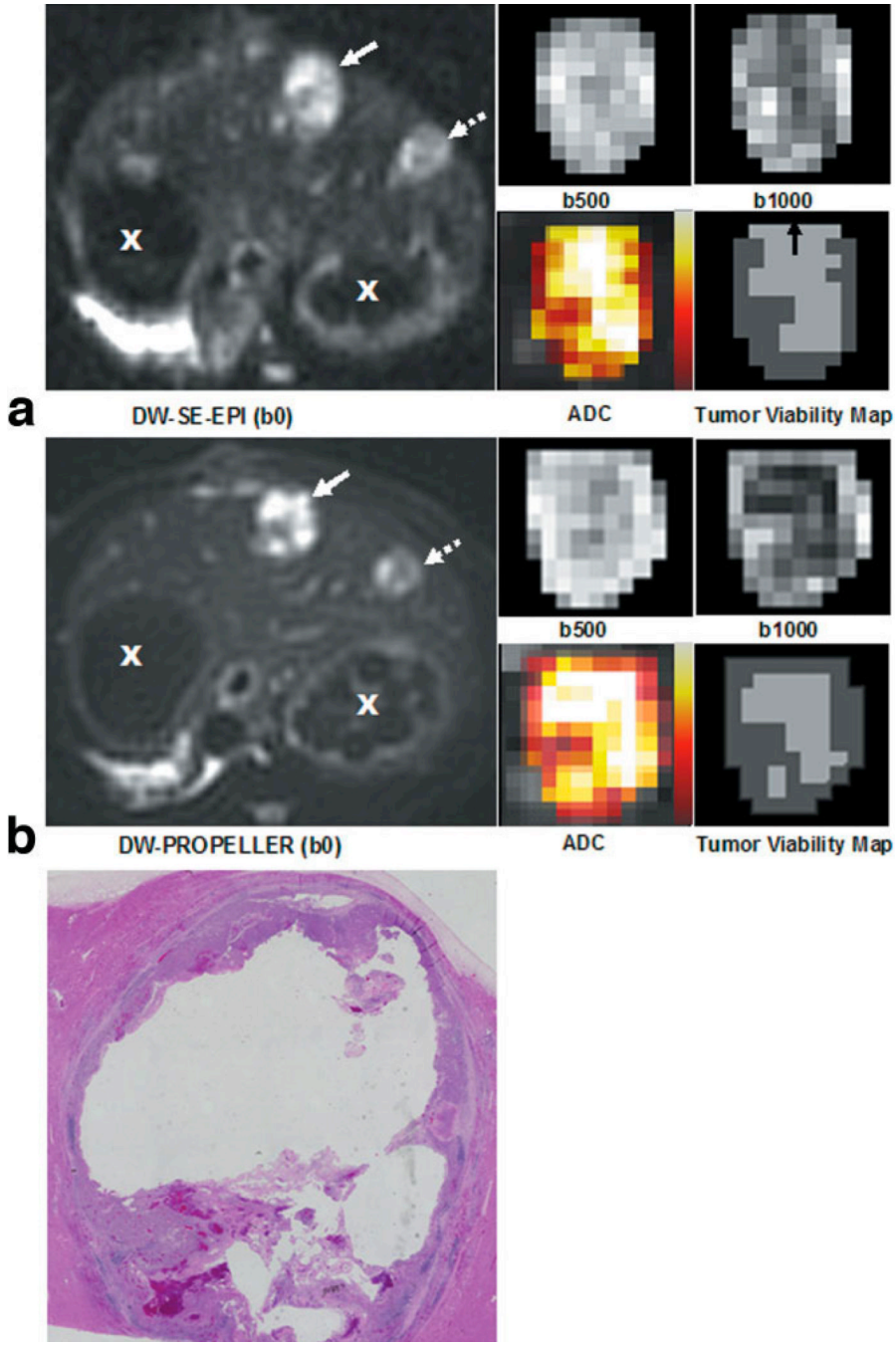

Figure 2.

Representative full FOV DW-SE-EPI (**a**) and DWPROPELLER (**b**) images (b = 0 s/mm^2), magnified tumor ROI DW images at b = 500 s/mm^2 and b = 1000 s/mm^2, and color-coded ADC maps fused to coregistered b = 0 images (scaled from bright colors representative of higher ADC values to darker colors representative of lower ADC values). Solid arrow indicates the tumor depicted in the magnified views while dashed arrow depicts the position of a smaller additional tumor and X indicates cross-sections of the stomach. Viable tumor tissues demonstrated increased signal intensity on DW images and decreased ADC relative to necrotic tissues with decreased signal intensity and increased ADC. Within each spatially resolved tumor viability map at lower right, the dark gray regions were classified as viable

tissues, whereas light gray regions were classified as necrotic tissues. These spatially resolved DW-PROPELLER viability maps demonstrated good correlation to corresponding H&E histology image (**c**) from the same axial slice position. Notice that due to blurring along the anterior–posterior orientation the DW-SE-EPI tumor viability map overestimated necrotic regions within anterior positions in the tumor (indicated by the black arrow on DW-SE-EPI tumor viability map).

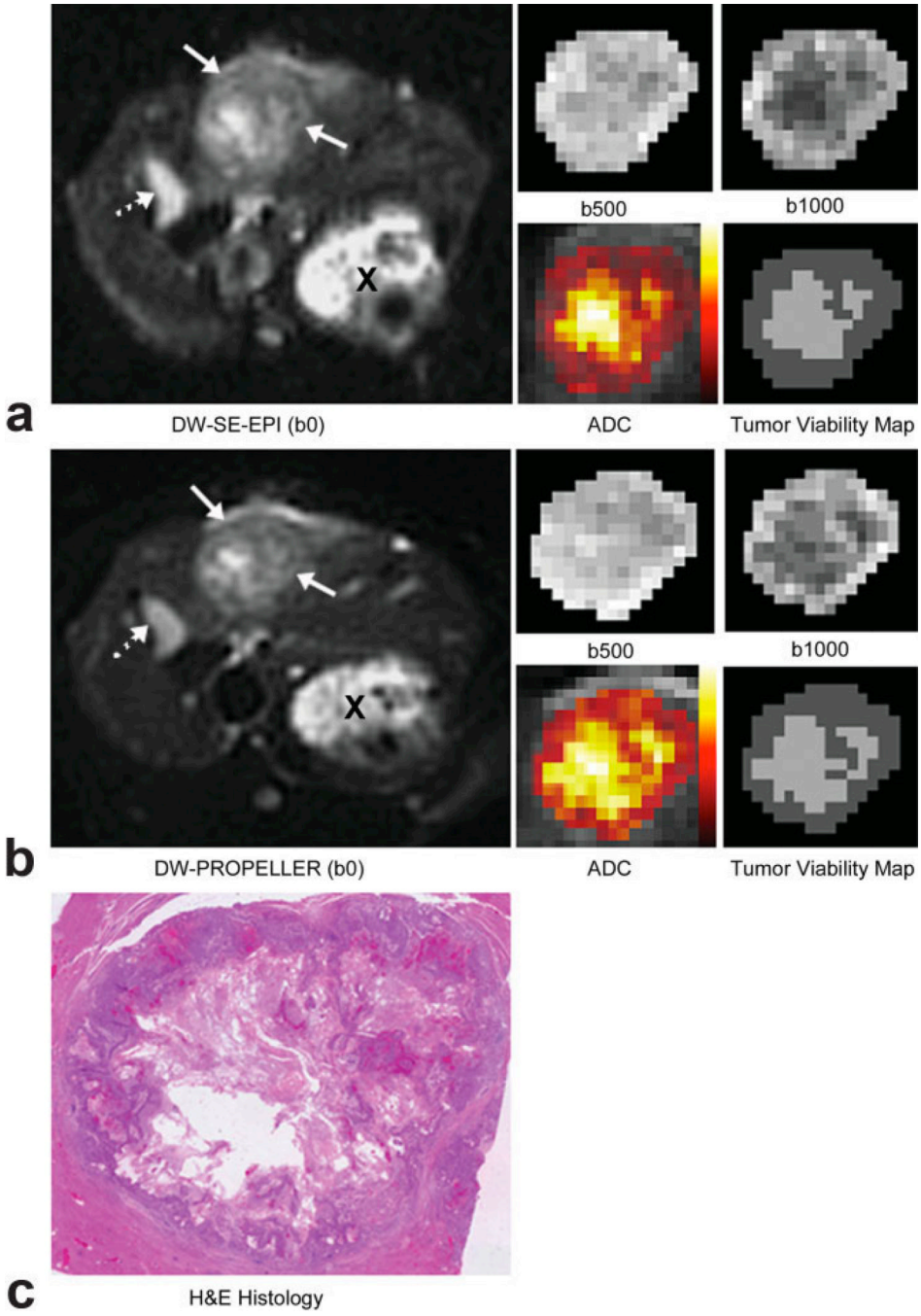

Figure 3.

Representative full FOV DW-SE-EPI (**a**) and DWPROPELLER (**b**) images (b = 0 s/mm^2), magnified tumor ROI DW images at b = 500 s/mm^2 and b = 1000 s/mm^2, and color-coded ADC maps fused to coregistered b = 0 images (scaling similar to Fig. 2). Solid arrows indicate tumor position while a dashed arrow indicates the position of the gallbladder and X indicates a cross-section of the stomach. Viable tumor tissues demonstrated increased signal intensity on DW images and decreased ADC relative to necrotic tissues with decreased signal intensity and increased ADC. Within each spatially resolved tumor viability map at lower right the dark gray regions were classified as viable tissues, whereas light gray regions were classified as necrotic tissues. Both DW-SE-EPI and DWPROPELLER images clearly

differentiated tumor regions and intratumoral tissues. Spatially resolved viability maps demonstrated good correlation to corresponding H&E histology image (**c**) from the same axial slice position.

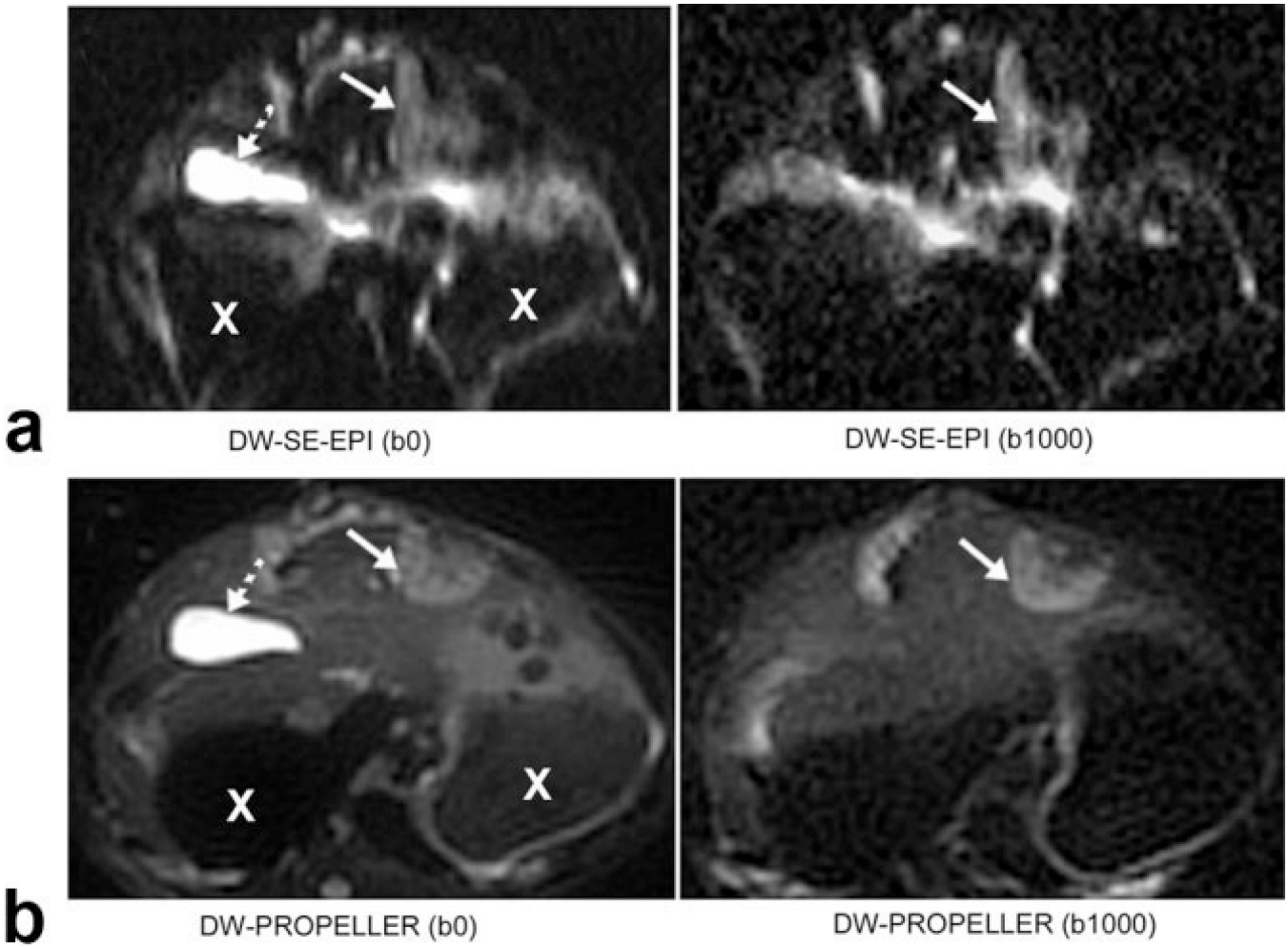

Figure 4.
Specific example demonstrating severe distortion within DW-SE-EPI images (top row) clearly mitigated using the DW-PROPELLER approach (bottom row). Solid and dashed arrows indicate VX2 tumor positions and gallbladder positions, respectively. X indicates a cross-section of the stomach.

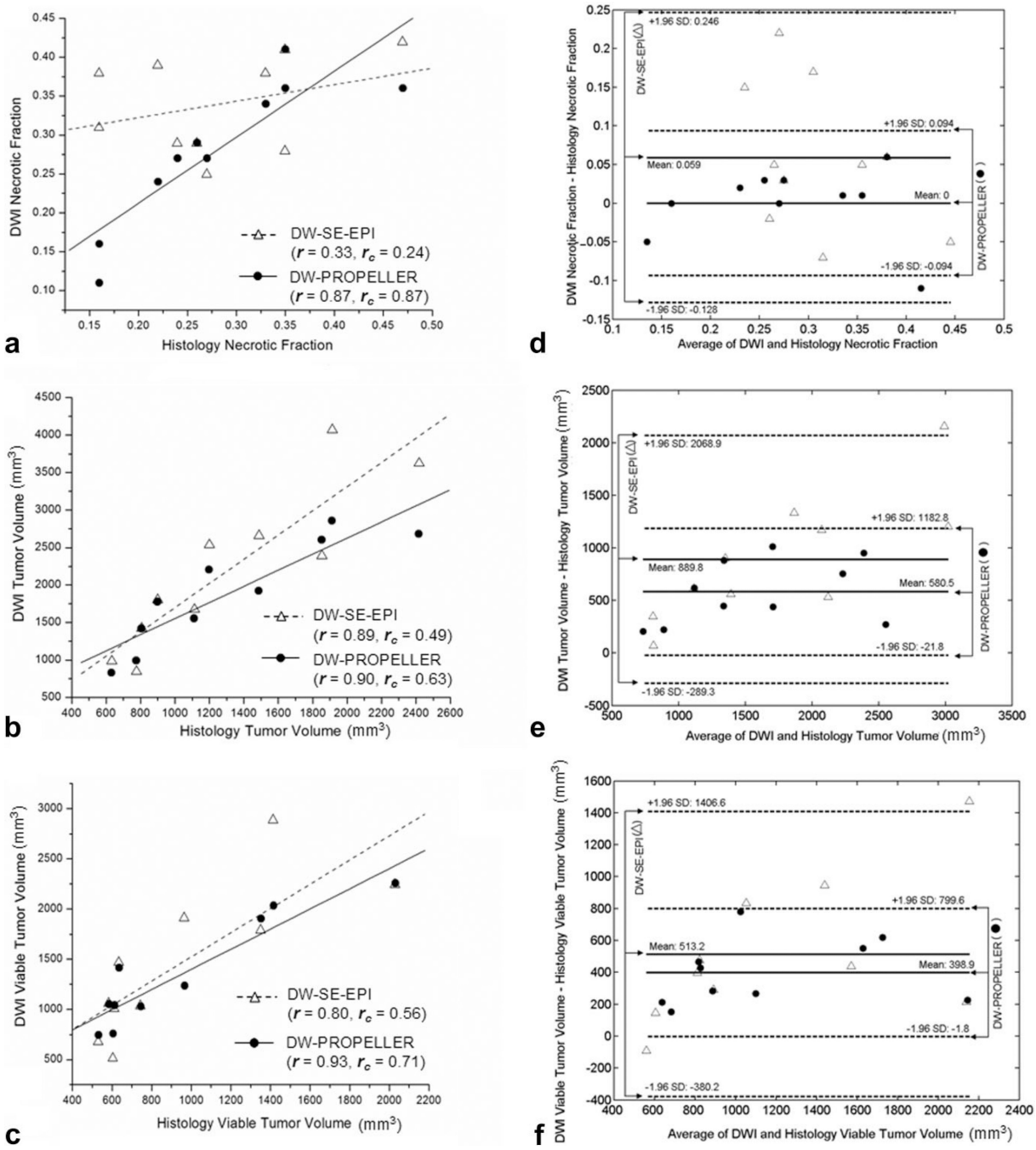

Figure 5.

Correlation (*r*: correlation coefficient), concordance (r_c: concordance coefficient) (a–c) and the Bland–Altman (d–f) analysis of DW-SE-EPI and DW-PROPELLER necrotic fraction (a,d), whole tumor volume (b,e), and viable tumor volume (c,f) measurements to corresponding reference standard histology measurements in 10 VX2 rabbit liver tumors. Bland–Altman plots showed the difference vs. average of DWI and histology measurements in each tumor with the mean differences (solid lines) and limits of agreement (mean ± 1.96 SD, dashed lines).